A principal components/singular spectrum analysis approach to ENSO and PDO influences on rainfall in western Iran

Monireh Biabanaki, Seyed Saeid Eslamian, Jahangir Abedi Koupai, Julio Cañón, Giorgio Boni and Mahdi Gheysari

ABSTRACT

This paper analyzes the spatio-temporal variability of precipitation in western Iran by means of the Standardized Precipitation Index (SPI), calculated in annual and seasonal aggregations for wet and dry conditions over 46 synoptic stations with monthly data from 1957 to 2008. Regions of homogeneous SPI realizations were delimited using principal components analysis (PCA) to highlight major variation modes distinguishable in the basin and singular spectrum analysis (SSA) was performed over the reconstructed values of SPI to identify their oscillation modes. Extreme SPI values associated with El Niño–Southern Oscillation (ENSO) and Pacific Decadal Oscillation (PDO) were also evaluated. Results show two significant oscillations around 4 and 8 years on the SPI with an increase in precipitation variability since 1990 and a tendency to have less rain during the cold season and more rain during the warm season. We calculated standardized products among SPI, ENSO, and PDO to determine years in which the indices reinforce each other, 1986, 1992, 1999, and 2008 being particularly significant in the associations. These results are important for water managers in western Iran because they indicate significant changes in precipitation regimes associated with ENSO and PDO signals that will help to assess the occurrence of droughts and floods in the area.

Key words | ENSO, Iran, PDO, singular spectrum analysis, spatio-temporal analysis, SPI index

Monireh Biabanaki (corresponding author)
Seyed Saeid Eslamian
Jahangir Abedi Koupai
Mahdi Gheysari
Water Engineering Department, College of Agricultural,
Isfahan University of Technology,
Isfahan, 8415683111,
Iran
E-mail: *biabanaki@yahoo.com*

Julio Cañón
School of Environmental Engineering,
Grupo GAIA, Universidad de Antioquia,
Medellin,
Colombia

Giorgio Boni
University of Genoa,
Via Balbi, 5,
16126 Genoa,
Italy

INTRODUCTION

Iran, which belongs to the arid/semi-arid zone of Asia and receives less than a third of the world's average precipitation, has gradually shifted towards drier conditions (Ashouri *et al.* 2008). This shift implies the need to study the variability of precipitation in the country, especially in terms of severe drought conditions. The variation of rainfall is very high between years, thus the country sometimes experiences drought. Rainfall varies both temporally and spatially. In general, most of the relatively scarce annual precipitation falls from October to April (Eslamian *et al.* 2009).

A coupled atmosphere–ocean system may provide a climatic insight into the mechanisms that can strongly affect the magnitude and also the distributions of precipitation in the region. The understanding and quantification of the relationship between regional climate anomalies and large-scale circulation drivers have been a hot topic of research worldwide. The El Niño-Southern Oscillation (ENSO) phenomenon over the tropical Pacific and also the Pacific Decadal Oscillation (PDO) are quite important because of their huge impacts on hydro-meteorological disasters like floods and droughts. The influence of ENSO on climate in the Asia/Pacific region and the influence of the North Atlantic Oscillation (NAO) on climate in Europe, in particular, have drawn much attention in recent years (Zhang *et al.* 2007; Gelati *et al.* 2011; Wrzesiński & Paluszkiewicz 2011; Chen & Hong 2012; Parry *et al.* 2012; Skaugen *et al.* 2012).

While some efforts have been made to study the precipitation variability in Iran (Domroes *et al.* 1998; Dinpashoh

doi: 10.2166/nh.2013.166

et al. 2004; Soltani & Modarres 2006; Soltani & Gholipoor 2006; Raziei & Azizi 2007; Ashouri et al. 2008), no comprehensive study on extreme rainfall conditions (i.e., deviation of actual precipitation from a historically established norm), supported by a standardized drought index and by spectral analysis (focused on atmosphere–ocean phenomena), has been performed for western Iran.

In this study we perform point frequency analysis and principal component analysis (PCA) to examine patterns of precipitation variability in western Iran at seasonal and annual aggregations and analyze how these extreme patterns may be influenced by ENSO and PDO. PCA is useful to reduce the dimensionality of spatially distributed time series of precipitation and to interpret spatial patterns, from a statistical viewpoint, through the distribution of significant eigenvectors that explain an important fraction of the series variability (Huth 1999; Wheater et al. 2005; Novembre & Stephens 2008). Moreover, PCA can be used to detect trends and changes of variability in hydrologic time series (Muchoney & Haack 1994; Smith et al. 2007; Tomassini & Jacob 2009).

We evaluated precipitation from 46 rain gauges in terms of the Standardized Precipitation Index (SPI) aggregated seasonally and annually. To determine temporal changes in precipitation variability we performed singular spectrum analysis (SSA), a non-parametric statistical tool that allows the separation of different components in the time series, such as trends and periodicities or oscillations, according to the variance that each component is able to explain in the series (Elsner & Tsonis 1996; Golyandina et al. 2001; Moskvina & Zhigljavsky 2003). SSA is used commonly in the analysis of climatic and meteorological time series (Peters et al. 2006; Jawson & Niemann 2007).

Finally, we determine which years of the available record (1957–2008) were relatively more affected by ENSO and PDO using a standardized year-by-year product among the indices that highlight only those extreme years where the signals highly reinforce each other.

DATA SOURCES

Study area

Western Iran covers the region between 33 and 39 degrees latitude north and 45 and 52 degrees longitude east, as shown in Figure 1. The region is mostly occupied by the Zagros Mountain range, which faces the direction of the prevailing moisture bearing systems (Domroes et al. 1998; Dinpashoh

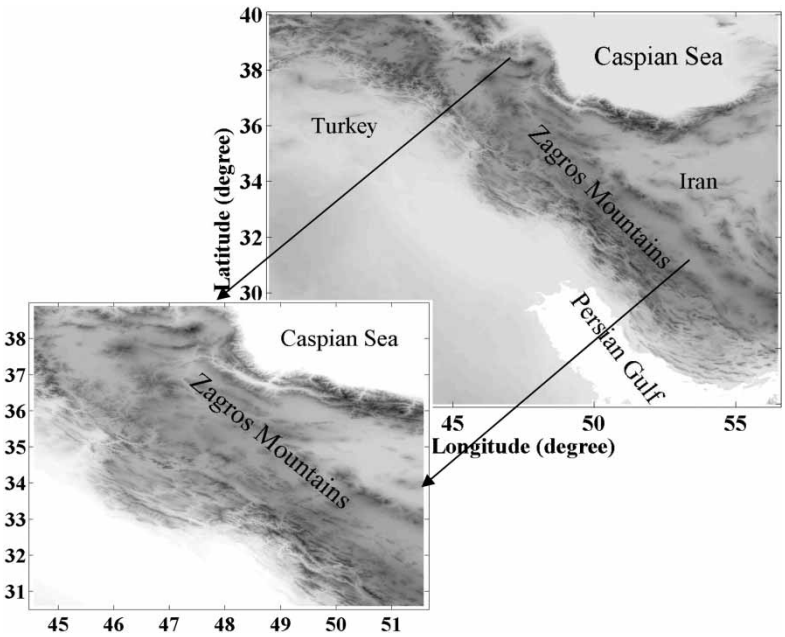

Figure 1 | Study area in western Iran.

et al. 2004). Due to the latitudinal extent and its complex relief, the precipitation amount varies greatly over the region.

Precipitation data

This study analyzes monthly precipitation data from 52 synoptic stations (covering the period from 1957 to 2008, which is the last date available from Iran Meteorological Organization database). We tested the data for randomness purposes using the run test with binomial distribution, which is used to decide whether or not a dataset is random (a sorted series of increasing values is considered random when the probability of the $[i+1]$th value being larger than the $[i]$th value follows a binomial distribution). Six stations did not have sufficient and random data, so the other 46 stations were selected. A scatter plot showing the location of these stations, their elevations, and the annual precipitation (from 1957 to 2008) for each station are shown in Figure 2.

The average of annual, maximum, and minimum precipitation values are shown in Figure 3(a). The seasonal precipitation plots, defined by the cold season (October to April, Figure 3(b)) and the warm season (May to September, Figure 3(c)), also include the percentage of total precipitation per station that occurs in each respective season. Precipitation during the cold season represents more than 50% of total annual precipitation in all stations. During the warm season precipitation is higher towards the north, but during the cold season tends to be evenly distributed over the area with some high values towards the south and west. The values in both seasons tend to be uniform at the center of the study area.

PDO and BEST data

PDO time series

This study uses the monthly standardized values for the PDO index (Mantua 2000). The PDO appears to oscillate

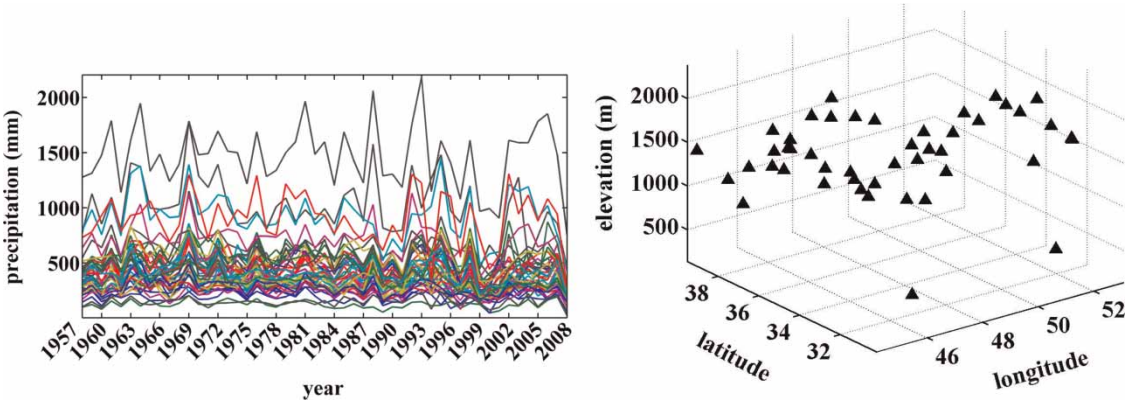

Figure 2 | Left: Annual precipitation at each station. Right: Location and elevation of synoptic stations used in this study.

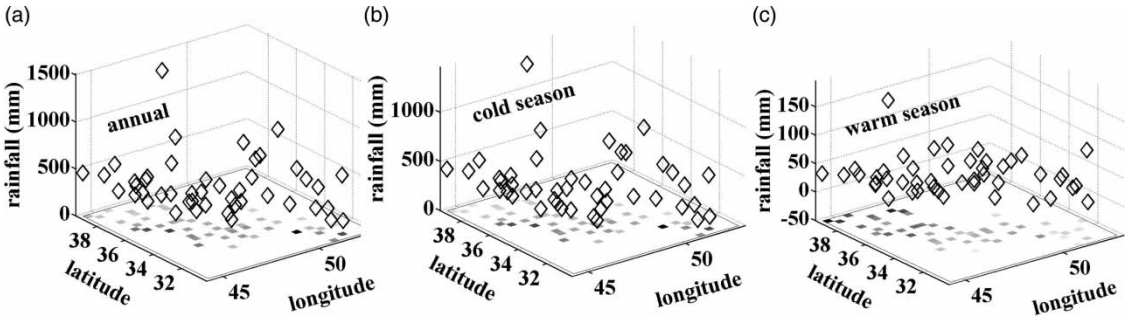

Figure 3 | (a) Average of annual, maximum, and minimum precipitation (mm) at the stations; (b) cold season's mean precipitation and percentage of total precipitation; (c) warm season's mean precipitation and percentage of total precipitation.

between warm and cool phases every 20 to 30 years (Null 2002). The negative, cool phase has occurred in 1900 to 1924, 1947 to 1976, and 1998 to the present. The rest of the period corresponds to the positive, warm phase. This monthly time series is available at: http://jisao.washington.edu/pdo/PDO.latest.

BEST time series

The bivariate ENSO time series (BEST) index was designed to be simple to calculate and to provide a long-term ENSO index for research purposes. Nino 3.4 has traditionally been used as a measure of ENSO strength in the tropical Pacific. The time series is based on combining an atmospheric component of the Southern Oscillation Index (SOI) with an oceanic component (Nino 3.4 SST which is defined as the SST averaged over the region 5N to 5S and 170 to 120 W) (Smith & Sardeshmukh 2000). This time series is available at NOAA (http://www.esrl.noaa.gov/psd/data/correlation/censo.data). The BEST index has been used to relate the behavior of different hydrologic variables with ENSO (Cañón *et al*. 2007; Bookhagen & Strecker 2010).

METHODOLOGY

Our study begins with the analysis of the spatial and temporal variability of precipitation quintiles in terms of the SPI by means of the point frequency analysis of the coverage of abnormally wet and dry conditions and the derivation of significant Empirical Orthogonal Functions (EOFs) over the study area. The study proceeds to identify the existence of consistent common oscillatory modes of SPI via the application of SSA. Finally, an index product is proposed to detect extremely wet and dry conditions significantly associated with the interactions between the three signals (SPI, PDO, and ENSO). The work is based on aggregations of the indices in water years (from October to September) and seasonal aggregations in two periods, the cold season (October to April) and the warm season (May to September).

The SPI is an index based on the probability of precipitation for different time scales, representing processes that go from those rapidly affected by atmospheric behavior (weeks or months) to effects at scales of seasons and years (Moreira *et al*. 2008). SPI has been used in several countries around the world for the analysis and assessment of droughts (Patel *et al*. 2007).

The SPI series in this study are grouped in annual and seasonal sets. The seasonal SPI compares the precipitation of the season in different periods over the historical record. The seasonal SPI indicates medium-term trends in precipitation that may affect stream flows and reservoir levels.

The annual (12-month) SPI is a comparison between consecutive 12-month cumulative precipitation values throughout the historic record. The annual SPI reflects long-term interannual precipitation patterns. According to Hayes *et al*. (2000), annual SPI values are probably tied to stream flows, reservoir levels, and even groundwater levels at longer time scales.

The SPI is computed by fitting a gamma probability density function (PDF) to a given frequency distribution of precipitation summed over the time scale (1957–2008). This is performed at each station separately for the cold season, warm season, and water year (October to September). Each PDF is then transformed into the standardized normal distribution (Lloyd-Hughes & Saunders 2002). These series were analyzed in their spatial distribution and temporal recurrence using PCA and SSA, respectively. A brief description of the procedure is presented in the following two sections.

Spatial analysis using PCA

PCA is a linear optimization method that maximizes the explained variance of a dataset by decomposing the original series in an orthogonal set of eigenvectors (EOFs). In this study, the spatial variability of annual and seasonal SPI datasets was analyzed via the distribution of their significant eigenvectors.

A Monte Carlo generation process of 100 correlation matrices of independent random variables with mean zero and unit variance (similar to the SPI parameters) was performed to account for the effects of white noise. The random matrices were decomposed in their singular values and sorted in decreasing order of variance explained.

Only the eigenvalues that are above the white noise threshold are considered to be significant. The SPI matrix can then be partially reconstructed using only the significant

eigenvectors. To reduce the effects of domain-shape dependence a varimax rotation was also applied to the significant eigenvectors. The coefficients of the rotated significant eigenvectors for the annual and seasonal series were plotted over the stations and their spatial distributions were analyzed to identify possible patterns of SPI variability in the region.

Frequency analysis

The SSA approach is a useful non-parametric technique of time series analysis that has been widely used in hydrology to relate low frequency changes in temperature and precipitation associated with climate signals such as ENSO and PDO (Santos *et al.* 2006). SSA allows the original series to be decomposed into a small number of independent components that can be interpreted in terms of slowly varying trends, oscillatory components and a structure that is different from red noise. Detailed mathematical descriptions of the methods presented in these sections can be found in Ghil *et al.* (2002), Shun & Duffy (1999), and Hassani (2007). The code used in this study to perform SSA was written in Matlab®.

RESULTS AND DISCUSSION

We first discuss the spatial and temporal distribution of annual and seasonal SPI values within the area of study, relative to the occurrence of abnormally dry and wet events over each point of the grid, followed by the analysis of the linear transformation of point SPI time series into a reduced set of principal components (PC-SPI), the analysis of the spatial distribution of the significant EOFs and the identification of multiannual frequency oscillation modes in the PC-SPI values. Finally, we discuss the association of extreme events with the PDO and ENSO signals in the area of study.

Spatial and temporal incidence of abnormally wet and dry conditions

Following the methodology proposed by Cañón *et al.* (2007), the annual and seasonal occurrences of abnormally dry and wet conditions over western Iran were determined for absolute SPI values higher than 1.5, which are regarded as severe moisture conditions (classification proposed by McKee *et al.* (1993)).

The 1957–2008 cumulative frequency distributions (CDFs) of area covered by $|SPI| > 1.5$ are shown in Figure 4 for the case of the entire study area and three different aggregation periods: annual (October–September), cold season (October–April), and warm season (May–September). Values corresponding to El Niño and La Niña years are highlighted in Figure 4.

Results show that mostly dry events would be expected in western Iran during La Niña years, whereas wet and dry events are equally likely to occur during El Niño years. Although not all El Niño and La Niña years exhibit the same coverage of abnormal moisture conditions, the most severe and extended events are associated with ENSO years and lower or higher than normal PDO values. This result is indicative of the influence of both ENSO and PDO in the occurrence of severe regional moisture conditions in the area. The analysis also shows that the warm season tends to have less extreme events than the cold season for both wet and dry events.

PCA over spatially distributed SPI time series

The significant eigenvectors derived from PCA over the SPI (PC-SPI) for water year and seasonal series are shown in Figure 5. The spatial distributions of the varimax rotated components of significant eigenvectors are shown in Figure 6. The PCA applied to the annual SPI shows four eigenvectors significantly different from white noise (Figure 5). These four eigenvectors explain 89.4% of the variance.

The window length (L) is a key parameter in the decomposition stage of SSA. L should be large enough to identify low periodicities but not greater than half the length of the original series ($N/2$). In this study, the value of L was chosen from the results of w-correlation calculated for reconstructed series over different window lengths. Table 1 shows the results obtained for w-correlation from the simulated water year series with different L. A w-correlation of zero means that the components are separable. Results indicate that the minimum value of w-correlation

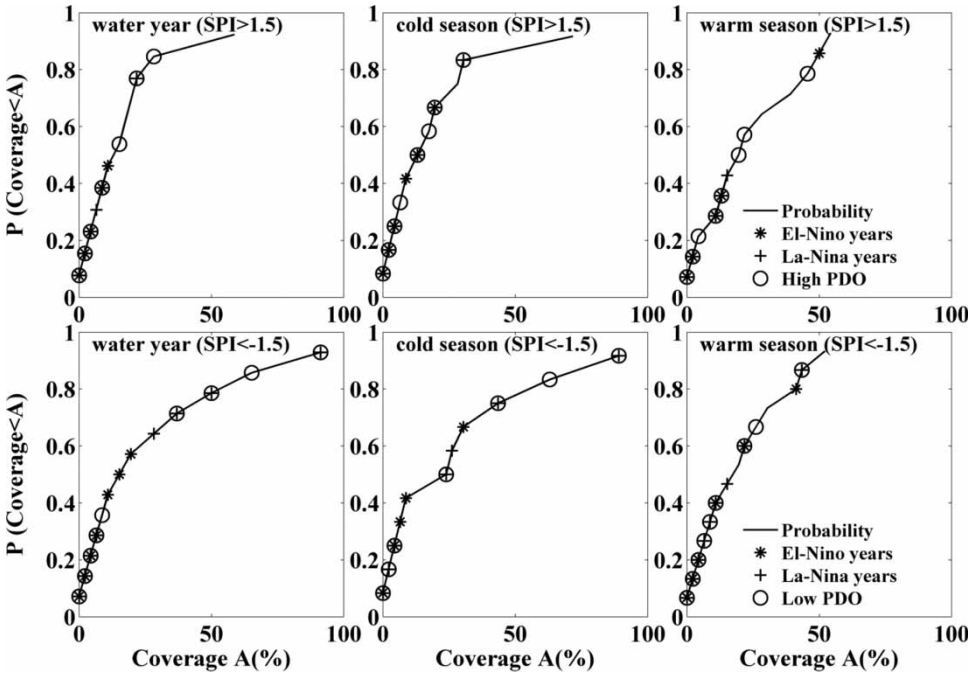

Figure 4 | CDF of area (A) covered by abnormally wet (upper row) and dry (lower row) moisture conditions.

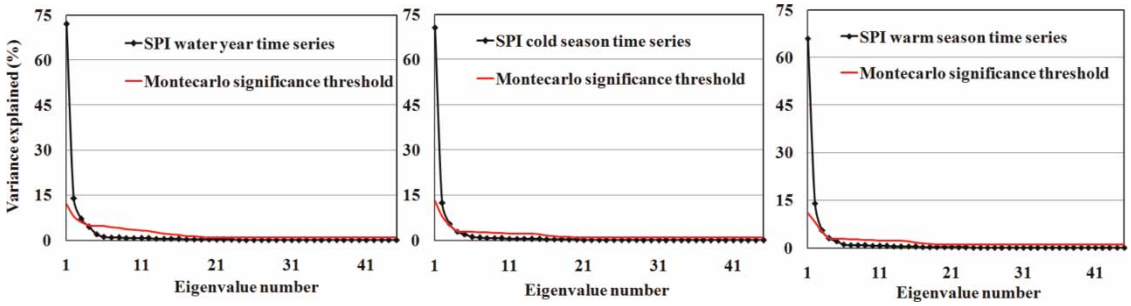

Figure 5 | Cumulative variance explained by eigenvalues for water year time series.

is obtained for the maximum value of the window length $L = N/2 \sim 25$ years (the time series length is equal to 51 years, from 1957 to 2008). Thus, we had 25 eigentriples in the decomposition stage (for more information, see Hassani *et al*. (2012)).

Regarding the SPI for water years (Figures 6(a1) to 6(a4)), the loadings of the first rotated EOF, explaining 72% of the variance, are not evenly distributed over the study area and have their major influence towards the south-east. The loading of the second rotated eigenvector, which explains approximately 14% of the variance, is noticed in the central part of the study area. The third and fourth rotated eigenvectors, which together explain 11.4% of the variance, show loadings oriented more towards the north with some influence over the upper and lower and center of the area. Although the fourth EOFs have a significant spatial coherence that was not detected in the EOFs derived from random processes, their distributions would still be conditioned by the shape of the domain.

For the cold season (Figures 6(b1) to 6(b4)), the loadings of the first rotated EOF (the more significant) explain 70.5% of the variance and are evenly distributed over the southern part of the study area. The second rotated eigenvector, which explains approximately 12.5% of the variance, is noticed in the northern part of the study area. The third rotated eigenvector, which explains 5.5% of the variance shows

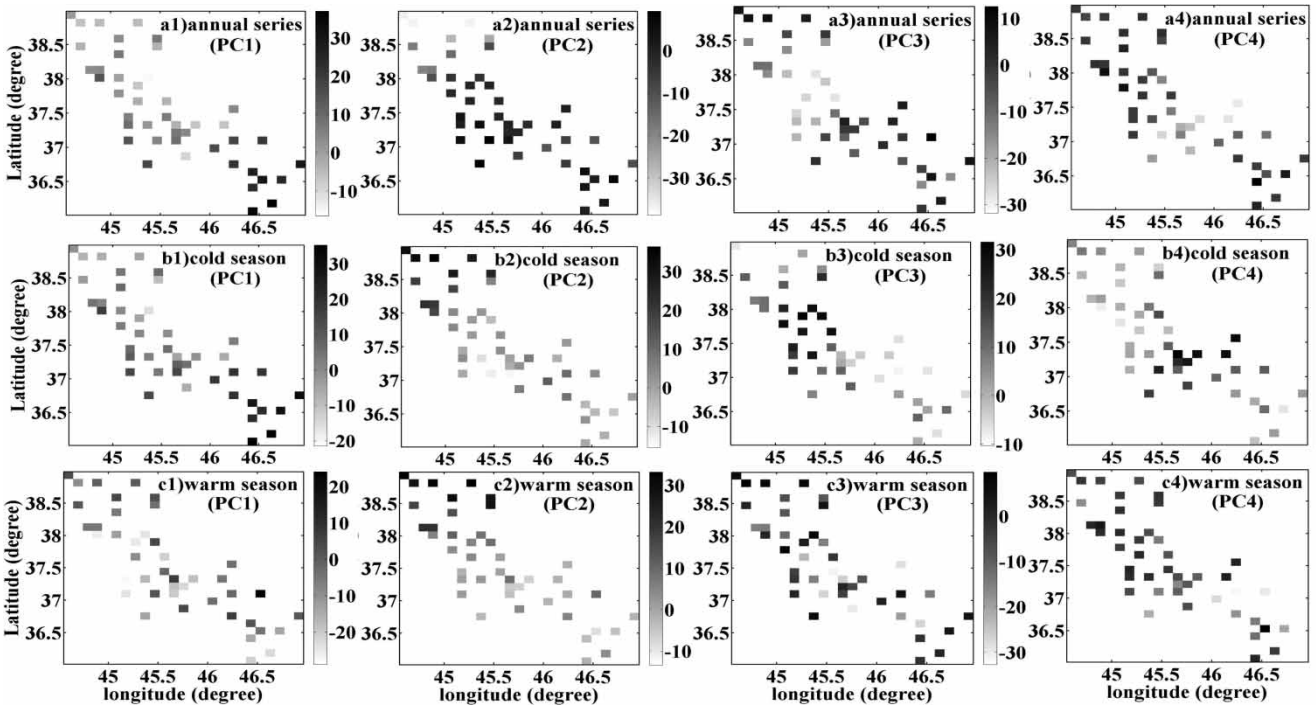

Figure 6 | Varimax rotated spatial distribution of the four significant EOFs for: annual mean precipitation ((a1) to (a4)), cold season's mean precipitation ((b1) to (b4)), and warm season's mean precipitation time series ((c1) to (c4)).

Table 1 | The value of weighted correlation for different values of window length (L) for reconstructed water year time series

Window length (L)	10	15	20	25
w-correlation	0.00263	0.00103	0.00046	0.00026

loadings oriented in the center part (near the north). The fourth rotated eigenvector (explaining 2.9% of the variance) shows loadings oriented in the center part of the study area.

Finally, for the warm season (Figures 6(c1) to 6(c4)), the first rotated EOFs explain 66% of the variance and also the third and fourth rotated eigenvectors, which together explain 8.5% of the variance, show loadings oriented in more or less all parts of area. The second rotated eigenvector, which explains approximately 14% of the variance, is noticed in the northern part of the study area.

The advantage of having identified these specific modes lies in the possibility of extracting a considerable amount of information from the study area using only a reduced set of principal components PC-SPI. Each PC-SPI represents a weighted average of the SPI over the basin. The vector sum of the first four PC-SPIs in turn provides a projected time series representing the variance explained by the rotated EOFs. This time series was used in the SSA to determine the presence of common oscillations.

SPI oscillation modes with SSA

The reconstructed PC-SPI time series was analyzed using SSA for the period 1957–2008 in order to identify consistent oscillatory modes.

Decomposition: window length and eigenvalues

The window length L is the only parameter in the decomposition phase (Hassani 2007). In this study, for water year and seasonal time series $L = 25$ has been used. Based on this window length and on the eigenvalues of the trajectory matrix (25×25), there are 25 eigentriples, ordered by their contribution (share) in the decomposition.

Figure 7 represents the PCs related to the first six eigentriples for water year, cold and warm seasons' time series.

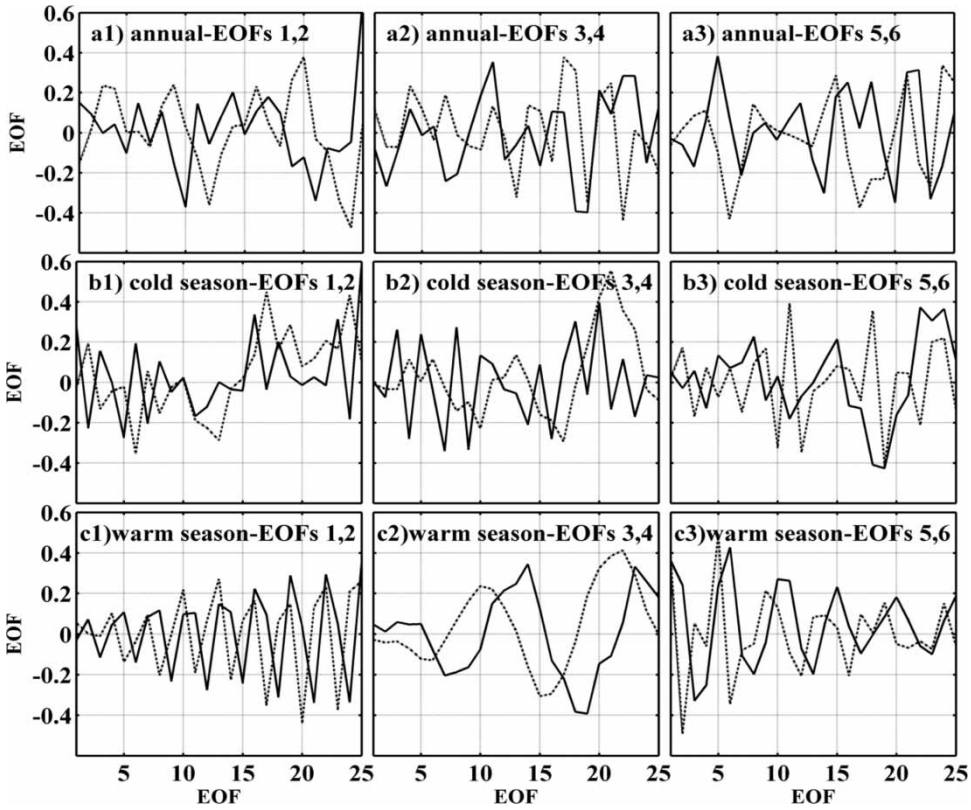

Figure 7 | EOFs related to the first six eigentriples for: (a1) to (a3) water year, (b1) to (b3) cold season, and (c1) to (c3) warm season time series.

Usually, every harmonic component with different frequency produces two eigentriples with close eigenvalues (except for frequency 0.5 which provides one eigentriple with saw-tooth singular vector). Another useful insight is provided by checking breaks in the eigenvalue spectra. As a rule, a pure noise series produces a slowly decreasing sequence of singular values. Figure 8 shows the logarithms of 25 singular values for water year, cold and warm seasons, and PC-SPI time series for these periods.

Two evident pairs with almost equal leading singular values are related to two (almost) harmonic components of the annually PC-SPI series, eigentriple pairs 2–3, 4–5, and 6–7 are related to harmonics with specific periods, for water year and cold season time series and also eigentriple pairs 1–2, 3–4, and 5–6 for warm season time series (Golyandina *et al.* 2001, Chapters 1 and 2). Each PC-SPI represents a weighted average of the SPI over the region. The vector sum of the eigentriple pairs 2–3, 4–5, and 6–7 PC-SPIs for water

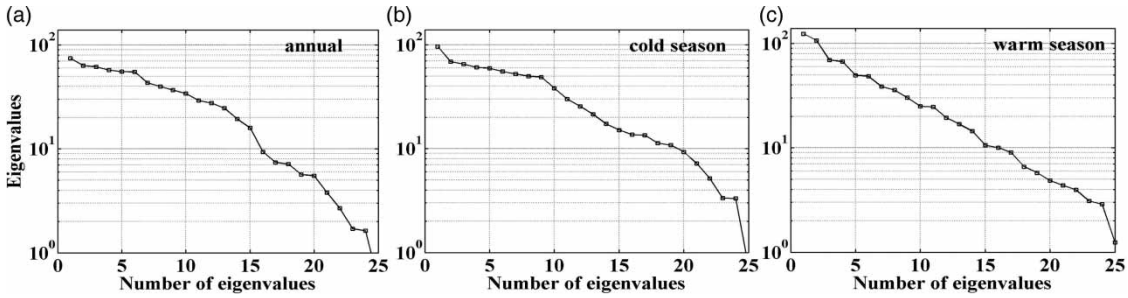

Figure 8 | Logarithms of 25 eigenvalues and PC-SPI time series for (a) water year, (b) cold season, and (c) warm season time series.

year and cold season time series and 1–2, 3–4, and 5–6 PC-SPIs for warm season, respectively, provides a projected time series representing the variance explained by the R-EOFs. These time series were used in the SSA to determine the presence of common multiannual oscillations in the data.

Pairwise scatter plots

The singular values of the two eigentriples of a harmonic series are often very close to each other, and this fact simplifies the visual identification of the harmonic components (Hassani *et al*. 2009). Figure 9 depicts scatter plots of the paired eigenvectors in the PC-SPI water year, cold and warm seasons' time series, corresponding to the harmonics with periods of 3 and 8 years (Hassani *et al*. 2009).

Reconstruction

Reconstruction stage includes two separate steps: grouping (identifying signal component and noise) and diagonal averaging (using grouped eigentriples to reconstruct the new series without noise). Usually, the leading eigentriple describes the general tendency of the series.

The SSA technique depends on the number of eigenvalues (r) that are important for separating signal components from a noisy reconstructed series of length N. Table 2 represents the results of reconstructed water year series with different r (1 to 5).

The reconstructed signal, considering w-correlation, variance, and root mean square error (RMSE) criteria, is calculated by using the first five eigenvalues and $L = 25$

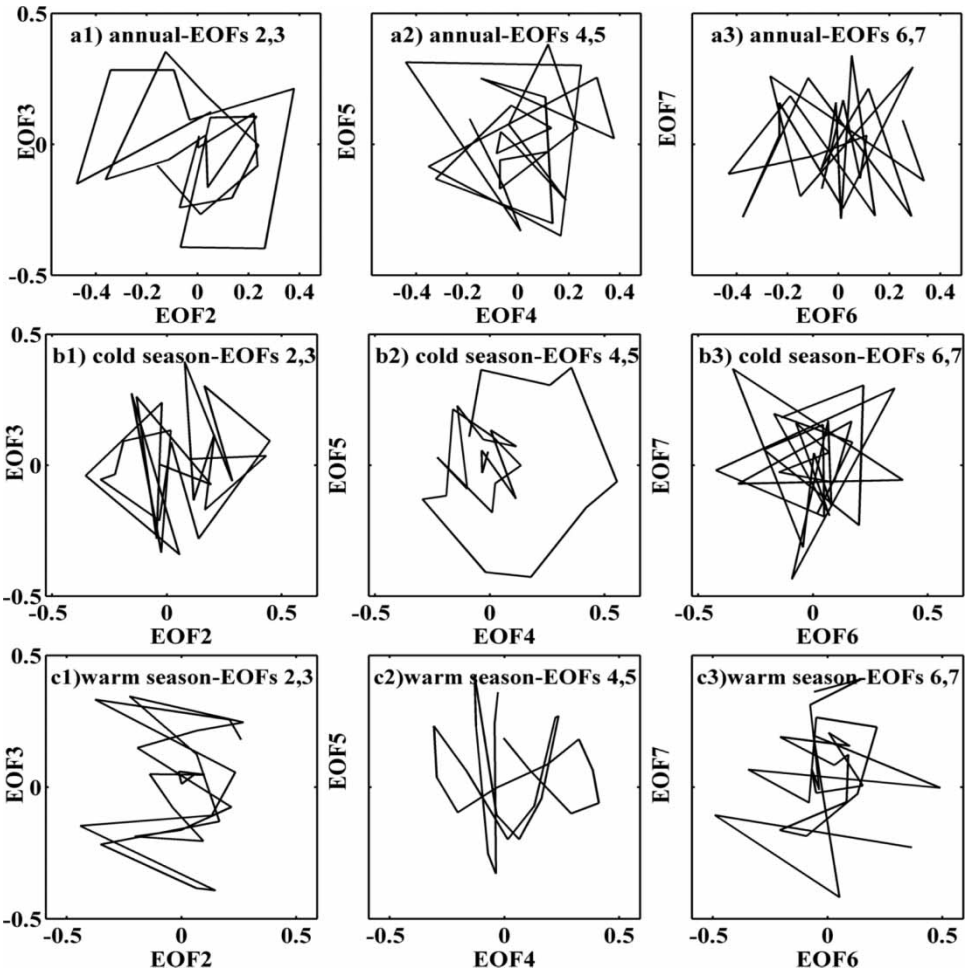

Figure 9 | Scatter plots of the paired harmonic eigenvectors for: water year (a1) to (a3), cold season (b1) to (b3), and warm season (c1) to (c3) time series.

Table 2 | The value of weighted correlation, variance, RMSE of the signal reconstruction step for water year time series with different values of *r*

Number of eigenvalues (*r*)	1	2	3	4	5
w-correlation	0.0056	0.0033	0.0025	0.0017	0.0016
Variance	0.2703	0.2426	0.2423	0.1532	0.1505
RMSE	0.7423	0.6992	0.6731	0.5915	0.5894

years. There is insignificant difference between the fourth and fifth eigenvalues due to their proximity in contribution. Thus, the first four eigenvalues can be used to reconstruct the noise-free signal from the water year series (for more information, see Hassani *et al.* 2012).

The sum of the reconstructed components derived from two pairs of significant eigenvectors indicate that the method tends to reconstruct better the last part of the series. The reconstructions are shown in the right part of Figure 10 for water year, cold and warm seasons. These results suggest a change in precipitation regime in western Iran, starting approximately in the mid-1990s, more noticeable when the seasonal series are reconstructed. This result is very important for water management policies in the study area. The change may be associated in part with ENSO and PDO positive and negative in phase oscillations with PC-SPI. This can also be observed in the standardized products among these indices, described below in Figure 11.

The reconstructions in Figure 10 show an off-phase behavior between the cold and warm seasons, the drier than average periods in the cold season usually being compensated by wetter than normal warm seasons and vice versa. This result is also important for water managers, since the analysis of the entire year may hinder the effects of seasonal extremes in the basin.

SPI extreme event associations with PDO and BEST

Based on the synchronic oscillation of the reconstructed SPI time series, standardized products among SPI and the indices PDO and BEST were calculated to explore the relative influence of these climate drivers in the occurrence of abnormal SPI moisture conditions year by year (Cañón *et al.* 2007):

$$P_t = \frac{\mathrm{PCSPI}_t \times I_t}{\sqrt{\sigma^2_{\mathrm{SPI}} \times \sigma^2_{\mathrm{I}}}} \quad I_t = \{\mathrm{BEST}, \mathrm{PDO}, \mathrm{BEST} \times \mathrm{PDO}\} \tag{1}$$

where P_t is the year t cross product, I_t represents the index (or set of indices) against which the PC-SPI is going to be compared at each year t, and σ is the standard deviation of the

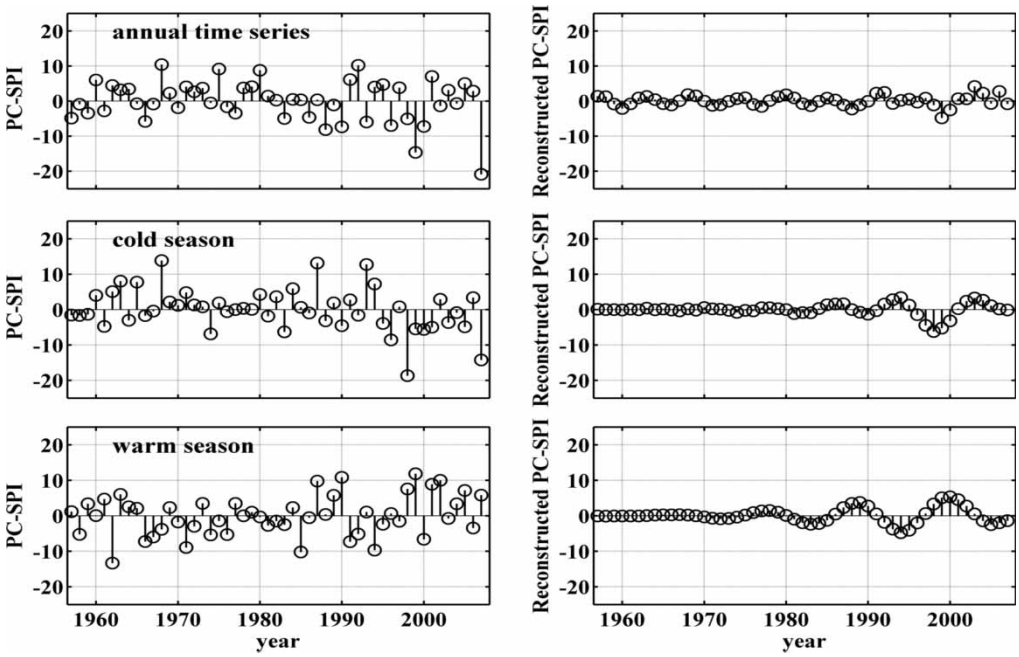

Figure 10 | Reconstructed series for water year, warm and cold seasons' time series.

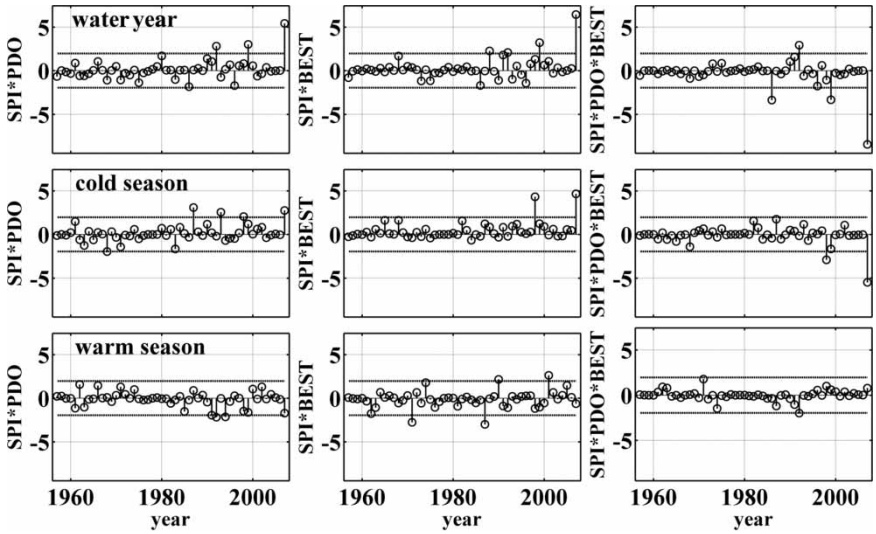

Figure 11 | Series of year-by-year standardized product of indices PC-SPI, ENSO, and PDO.

indices considered. The advantage of this year-by-year product of indices (normalized by the standard deviations) is that it allows us to observe the relative influence of ENSO and PDO on SPI values not at the level of the low frequency oscillations (like those that can be derived from SSA) but regarding the SPI of each particular year. In this way, we can generate time series of the products like those of Figure 11 and observe which particular years were more affected by the climate drivers.

Large positive (meaning equal direction) and negative (meaning opposite direction) products between the SPI and PDO, the SPI and BEST, and the SPI and both PDO and BEST in a particular year would indicate that the values are strong in the series and they reinforce each other whereas values close to zero would indicate a weak interaction of values. Due to the standardized nature of the indices, product values within ± 1.96 are considered normal conditions within the 95% confidence interval, whereas products out of this range are considered reinforcements.

Most of the time the products do not show any significant relationship between the SPI values and PDO (BEST) for water year, cold and warm seasons' time series, indicating either normal conditions in the basin or weak ENSO and PDO values. However, in certain years, the standardized product reveals strong reinforcing linkages between SPI and both PDO and BEST occurring at seasonal and water year aggregations (Figure 11). For instance, five of these reinforcements for water year time series coincide with years in which the SPI values were negative (1986, 1996, 1998, 1999, and 2008) and three of them coincide with years in which the SPI values were positive (1988, 1991, and 1992). The SPI-BEST product reveals a greater spread of extreme occurrences during the warm season whereas the SPI-PDO product shows more extreme years in the cold season. It can be seen that the extreme events are more frequent after 1990, especially during the cold season in which most of the precipitation in the basin occurs. La Niña years of 2008 and 1999 (which coincide with a negative phase of PDO), in particular, showed a marked reduction in precipitation in the region, with 2008 being the most extreme on record.

CONCLUDING REMARKS

In this research we have found that precipitation variability has been increasing over western Iran in the last two decades (since the mid-1990s). Furthermore, we found that ENSO and PDO may have a reinforcing effect on the occurrence of precipitation extremes (especially low values during negative phases of PDO and La Niña years), that occur region-wide and may be indicative of drought conditions, mainly during the cold season.

The use of SSA allowed us to detect an increase in precipitation variability since 1990. The SSA reconstructions reveal opposite phases between the cold and warm seasons, which indicates that wet warm seasons tend to be followed by dry cold seasons and dry warm seasons tend to be followed by wet cold ones. The point frequency study also shows that most of the abnormally dry and wet conditions over the study area have been related to ENSO and PDO extremes, where low phases of PDO during La Niña years relate to widespread dry events in both seasons, whereas wet events are not as significant in coverage but are related to a high phase of PDO. During El Niño episodes, we found that less widespread wet and dry conditions tend equally to occur. An inspection of the annual SPI shows that, in general, dry conditions were more persistent and widespread than wet conditions.

The product of the indices, which indicates specific years where SPI extremes are reinforced by the ENSO and PDO signals, shows also the increase in the number of reinforced years in the last two decades, mainly during the cold season (reflected also in the annual SPI). The warm season, by contrast, is more periodically affected by ENSO episodes but not by PDO ones. This product also suggests that La Niña years that occur during a negative PDO phase may produce extremely dry conditions in the area, a result to be taken into account in future assessments of droughts in western Iran.

Our main interest in this research was to analyze the variability of precipitation in western Iran associated with ENSO and PDO. We are aware that there is still an open debate concerning whether or not climate change influences these global climate signals. However, we consider that some of the results of this research (i.e., an increase in precipitation variability and the occurrence of extremely wet and dry years widely distributed in space) are linked with changes that have occurred in the past two decades that are likely related with the expected effects of climate change.

ACKNOWLEDGEMENTS

This research is based upon work supported by Isfahan University of Technology (Iran) and by CIMA Research Foundation (Italy). The authors thank the anonymous reviewers for their valuable comments that have helped improve the quality and clarity of the manuscript.

REFERENCES

Ashouri, H., Abrishamchi, A., Moradkhani, H. & Tajrishy, M. 2008 Assessment of Interannual and Interdecadal Climate Variability Effects on Water Supply in Zayandehrood River Basin, Iran. In: *The First International Conference on Water Resources and Climate Change*, Sultanate of Oman.

Bookhagen, B. & Strecker, M. R. 2010 Modern Andean rainfall variation during ENSO cycles and its impact on the Amazon drainage basin. In: *Amazonia, Landscape and Species Evolution: A Look into the Past* (C. Hoorn & F. Wesselingh, eds). Blackwell, Oxford, pp. 223–243.

Cañón, J., González, J. & Valdés, J. 2007 Precipitation in the Colorado River basin and its low frequency associations with PDO and ENSO signals. *J. Hydrol*. **333**, 252–264.

Chen, L.-H. & Hong, Y. T. 2012 Regional Taiwan rainfall frequency analysis using principal component analysis, self-organizing maps and L-moments. *Hydrol. Res*. **43** (3), 275–285.

Dinpashoh, Y., Fakheri-Fard, A., Moghaddam, M., Jahanbakhsh, S. & Mirnia, M. 2004 Selection of variables for the purpose of regionalization of Iran's precipitation climate using multivariate methods. *J. Hydrol*. **297**, 109–123.

Domroes, M., Kaviani, M. & Schaefer, D. 1998 An analysis of regional and intra-annual precipitation variability over Iran using multivariate statistical methods. *Theor. Appl. Climatol*. **61**, 151–159.

Elsner, J. & Tsonis, A. 1996 *Singular Spectrum Analysis: A New Tool in Time Series Analysis*. Plenum Press, New York.

Eslamian, S. S., Abedi-Koupai, J., Amiri, M. J. & Gohari, S. A. 2009 Estimation of daily reference evapotranspiration using support vector machines and artificial neural networks in greenhouse. *Res. J. Environ. Sci*. **3**, 439–447.

Gelati, E., Madsen, H. & Rosbjerg, D. 2011 Stochastic reservoir optimization using El Niño information: case study of Daule Peripa, Ecuador. *Hydrol. Res*. **42** (5), 413–431.

Ghil, M., Allen, R. M., Dettinger, M. D., Ide, K., Kondrashov, D., Mann, M. E., Robertson, A., Saunders, A., Tian, Y., Varadi, F. & Yiou, P. 2002 Advanced spectral methods for climatic time series. *Rev. Geophys*. **40** (1), 3.1–3.41.

Golyandina, N., Nekrutkin, V. & Zhigljavsky, A. 2001 *Analysis of Time Series Structure: SSA and Related Techniques*. Chapman and Hall, London.

Hassani, H. 2007 Singular Spectrum Analysis: methodology and comparison. *J. Data Sci*. **5**, 239–257.

Hassani, H., Heravi, S. & Zhigljavsky, A. 2009 Forecasting European industrial production with singular spectrum analysis. *Int. J. Forecast*. **25** (1), 103–118.

Hassani, H., Mahmoudvand, R., Zokaei, M. & Ghodsi, M. 2012 On the separability between signal and noise in singular

spectrum analysis. *Fluct. Noise Lett.* **11** (2), 1250014–1250025.

Hayes, M., Svoboda, M. & Wilhite, D. A. 2000 Monitoring drought using the standardized precipitation index. In: *Drought: A Global Assessment* (D. A. Wilhite, ed.). Routledge, London, pp. 168–180.

Huth, R. 1999 Statistical downscaling in central Europe: evaluation of methods and potential predictors. *Climate Res.* **13**, 91–103.

Jawson, D. S. & Niemann, J. D. 2007 Spatial patterns from EOF analysis of soil moisture at a large scale and their dependence on soil, land-use, and topographic properties. *Adv. Water Resour.* **30**, 366–381.

Lloyd-Hughes, B. & Saunders, B. A. 2002 A drought climatology for Europe. *Int. J. Climatol.* **22**, 1571–1592.

Mantua, N. J. 2000 PDO Index. Available at: http://jisao.washington.edu/pdo/ (accessed 5 December 2003).

McKee, T. B., Doesken, N. J. & Kleist, J. 1993 The relationship of drought frequency and duration to time scales. *Proceedings of the 8th Conference on Applied Climatology*, American Meteorological Society, Anaheim, CA, pp. 179–184.

Moreira, E. E., Coelho, C. A., Paulo, A. A., Pereira, L. S. & Mexia, J. T. 2008 SPI-based drought category prediction using loglinear models. *J. Hydrol.* **354**, 116–130.

Moskvina, V. & Zhigljavsky, A. A. 2003 An algorithm based on singular-spectrum analysis for change-point detection. *Commun. Stat. B-Simul.* **32**, 319–352.

Muchoney, D. M. & Haack, B. N. 1994 Change detection for monitoring forest defoliation. *Photogramm. Eng. Rem. S.* **60**, 1243–1251.

Novembre, J. & Stephens, M. 2008 Interpreting principal component analyses of spatial population genetic variation. *Nat. Genet.* **40**, 646–649.

Null, J. 2002 El Niño has a weather-making partner: Pacific Decadal Oscillation. In: *San Jose Mercury News*, 17 December.

Parry, S., Hannaford, J., Lloyd-Hughes, B. & Prudhomme, C. 2012 Multi-year droughts in Europe: analysis of development and causes. *Hydrol. Res.* **43** (5), 689–706.

Patel, N. R., Chopra, P. & Dadhwal, V. K. 2007 Analyzing the spatial patterns of meteorological drought using SPI. *Meteorol. Appl.* **14**, 329–337.

Peters, E., Bier, G., van Lanen, H. A. J. & Torfs, P. J. J. F. 2006 Propagation and spatial distribution of drought in a groundwater catchment. *J. Hydrol.* **321** (1–4), 257–275.

Raziei, T. & Azizi, Gh. 2007 A precipitation based regionalization in western Iran using principal component analysis and cluster analysis. *Iran-Water Resour. Res.* **3** (2), 62–65.

Santos, J., Corte-Real, J. & Leite, S. 2006 Atmospheric large-scale dynamics during the 2004/2005 winter drought in Portugal. *Int. J. Climatol.* **27** (5), 571–586.

Shun, T. & Duffy, C. J. 1999 Low-frequency oscillations in precipitation, temperature and runoff on a west facing mountain front: A hydrogeologic interpretation. *Water Resour. Res.* **35** (1), 191–201.

Skaugen, T., Stranden, H. B. & Saloranta, T. 2012 Trends in snow water equivalent in Norway (1931–2009). *Hydrol. Res.* **43** (4), 489–499.

Smith, C. A. & Sardeshmukh, P. 2000 The effect of ENSO on the intraseasonal variance of surface temperature in winter. *Int. J. Climatol.* **20**, 1543–1557.

Smith, D., Cusack, S., Colman, A., Folland, C., Harris, G. & Murphy, J. 2007 Improved surface temperature prediction for the coming decade from a global climate model. *Science* **317**, 796–799.

Soltani, A. & Gholipoor, M. 2006 Teleconnections between El Nino/Southern Oscillation and rainfall and temperature in Iran. *Int. J. Agr. Res.* **1**, 603–608.

Soltani, S. & Modarres, R. 2006 Classification of spatio-temporal pattern of rainfall in Iran using a hierarchical and divisive cluster analysis. *J. Spat. Hydrol.* **6** (2), 1–12.

Tomassini, L. & Jacob, D. 2009 Spatial analysis of trends in extreme precipitation events in high-resolution climate model results and observations for Germany. *J. Geophys. Res.* **114**, D12113.

Wheater, H. S., Chandler, R. E., Onof, C. J., Isham, V. S., Bellone, E., Yang, C., Lekkas, D., Lourmas, G. & Segond, M.-L. 2005 Spatial-temporal rainfall modelling for flood risk estimation. *Stoch. Env. Res. Risk A.* **19**, 403–416.

Wrzesiński, D. & Paluszkiewicz, R. 2011 Spatial differences in the impact of the North Atlantic Oscillation on the flow of rivers in Europe. *Hydrol. Res.* **42** (1), 30–39.

Zhang, Q., Xu, C.-Y., Jiang, T. & Wu, Y. J. 2007 Possible influence of ENSO on annual maximum streamflow of Yangtze River, China. *J. Hydrol.* **333**, 265–274.

First received 4 October 2012; accepted in revised form 15 May 2013. Available online 3 July 2013